

# ADVANCED FUNCTIONAL MATERIALS

## Supporting Information

for *Adv. Funct. Mater.*, DOI: 10.1002/adfm. 201403669

Simultaneous Control of Light Polarization and Phase  
Distributions Using Plasmonic Metasurfaces

*Jianxiong Li, Shuqi Chen,\* Haifang Yang, Junjie Li, Ping Yu,  
Hua Cheng, Changzhi Gu, Hou-Tong Chen, and Jianguo  
Tian\**

## Supporting Information

### **Simultaneous Control of Light Polarization and Phase Distributions Using Plasmonic Metasurfaces**

*Jianxiong Li, Shuqi Chen\*, Haifang Yang, Junjie Li, Ping Yu, Hua Cheng, Changzhi Gu, Hou-Tong Chen, and Jianguo Tian\**

#### **Table of contents:**

1. Numerical simulations
2. The optical properties of rectangular nano-aperture
3. Anomalous refraction in the plasmonic metasurface
4. Simulation of the generation of vector beams

Figures S1 to S7

#### **Other Supplementary Material for this manuscript includes the following:**

Movies S1 to S3

#### **1. Numerical simulations**

All of our numerical simulations were performed using commercial software COMSOL Multiphysics based on the finite element method (FEM). The permittivity of gold is described by the Drude model, and the dielectric constant of silicon dioxide is 2.25. For the simulation of anomalous refraction, the super cell shown in Figure 3 has periodic boundary conditions in the  $x$  and  $y$  planes, and the waveguide ports boundary conditions on the other boundaries. For the simulation of the generation of the radially, angularly polarized beam and hybrid vector optical beam, the waveguide ports boundary condition was also employed as the incident light source, and perfectly matched layers were placed around the simulation domain to completely absorb the waves leaving the simulation domain.

#### **2. The optical properties of rectangular nano-aperture**

##### **Excitation of SPP standing waves in an MIM waveguide:**

When the normally incident light is polarized perpendicular to the major axis of a rectangular metal nano-aperture, SPP beams with a  $\pi$  phase difference can be excited at two sides of the nano-aperture and propagate to opposite directions at the metal-dielectric interface, as illustrated in **Figure S1a**. Part of the excited SPPs can transmit through the nano-apertures to the other side of the film and be coupled in the metal-insulator-metal (MIM) waveguide (termed gap plasmons), where SPP standing wave can be obtained due to interference. Figure S1b shows the electric field distribution of the SPP standing wave in the MIM waveguide. The wavenumber of the SPP in the MIM waveguide is  $k_{spp} = 2\pi n_{eff} / \lambda_{inc}$ , and  $n_{eff}$  is the effective refractive index of the MIM waveguide.

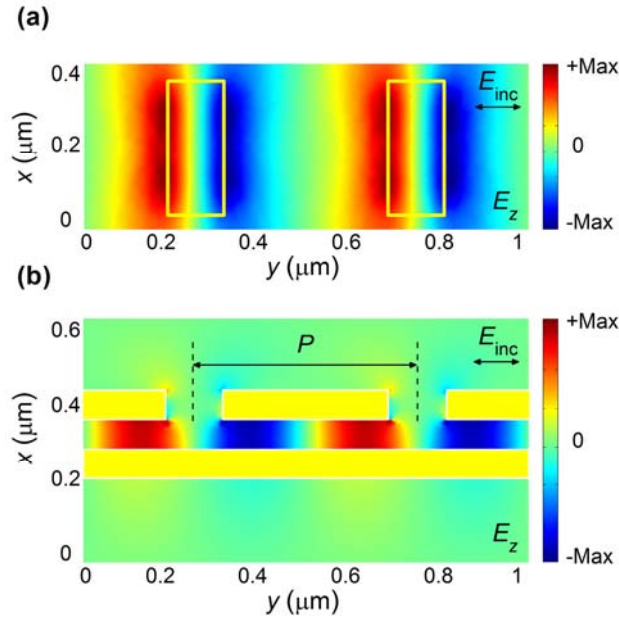


**Figure S1.** Simulated  $E_z$  field patterns of an MIM waveguide with periodic rectangular nano-apertures in the top metal film in (a) the  $x$ - $y$  plane and (b) the  $y$ - $z$  plane. The dimensions of the rectangular nano-apertures are the same as those in Figure 1. The incident light is linearly polarized along the  $y$ -axis at a wavelength of 900 nm.

### Out-coupling of SPPs in the MIM waveguide:

If the same rectangular nano-apertures are also inserted in the bottom metal layer, the SPPs propagating in the MIM waveguide can out-couple to free-space radiation, which generates the transmission light. The positions of the bottom rectangular nano-apertures will greatly affect the amplitude and phase of the transmission light. If the nano-apertures are located at the antinodes of the standing wave, the same kind of charges (either positive or negative) are excited within a bottom nano-aperture, resulting in inefficient out-coupling and low transmission. If the nano-apertures are located at the nodes of the standing wave, strong localized resonance and a large conversion from the SPPs to transmission light can be achieved, due to the excitation of opposite charges within a nano-aperture which results in efficient dipole radiation (together with the surface plasma resonance). The phase of the transmission light depends on the position of the bottom nano-aperture, which can be used to expand the tunable range of the phase. **Figure S2** shows the  $E_z$  field distributions of dual-layer rectangular nano-aperture film for  $S = 0$  and  $S = P/2$ , from which we can clearly observe the charge oscillations with opposite directions at the bottom nano-apertures, resulting in a phase difference of  $\pi$  for the transmitted light.

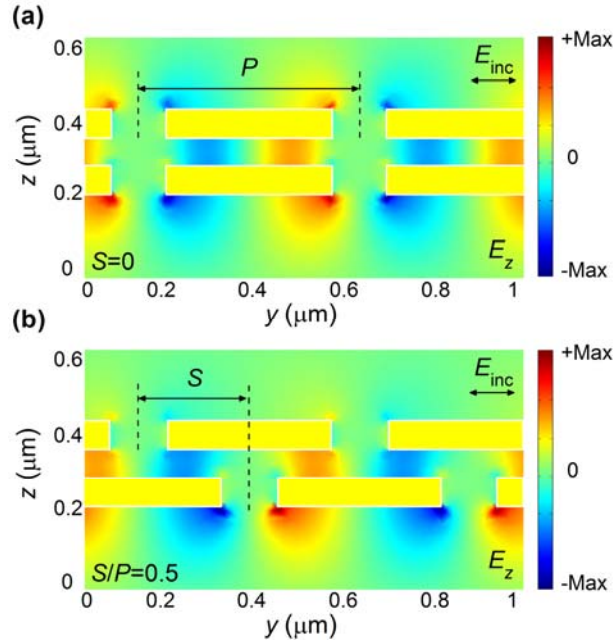


**Figure S2.** Simulated  $E_z$  field patterns of a dual-layer rectangular nano-aperture film in the  $y$ - $z$  plane for (a)  $S = 0$  and (b)  $S = P/2$ . The incident light is linearly polarized along the  $y$ -axis at a wavelength of 900 nm. The position of  $S = P/2$  corresponds exactly with the node of the standing wave.

#### Selective transmission of rectangular nano-aperture:

The rectangular nano-apertures in the metal film can selectively transmit light polarized perpendicular to their long axis because of the excitation of localized resonance as well as SPPs. Therefore, the polarization of the transmitted field completely depends on the orientation of the rectangular nano-aperture (together with different periods in  $x$  and  $y$  directions) under illumination by circularly polarized light. Plasmonic metasurfaces consisting of dual-layer rectangular nano-aperture film have the same characteristics as a single-layer rectangular nano-aperture film. **Figure S3** presents a plot of the simulated  $x$  and  $y$  components of the transmission amplitude for the aligned (laterally translated) plasmonic metasurface as functions of  $L$  and  $W$  with normally incident and circularly polarized light at 900 nm wavelength. This figure demonstrates that the six nano-apertures proposed in this work can only transmit the component of light polarized in the  $y$ -direction, which is vertical to the major axis of the rectangular nano-aperture. Note that the different periods in the  $x$ - and  $y$ -direction also contribute to the different SPP excitation and therefore the transmission. **Figure S4** shows the polarization selective transmission for two sub-units with small  $L/W$  ratio (less polarization selective) where the polarization selective transmission mainly results from the different periods in  $x$  and  $y$  directions.

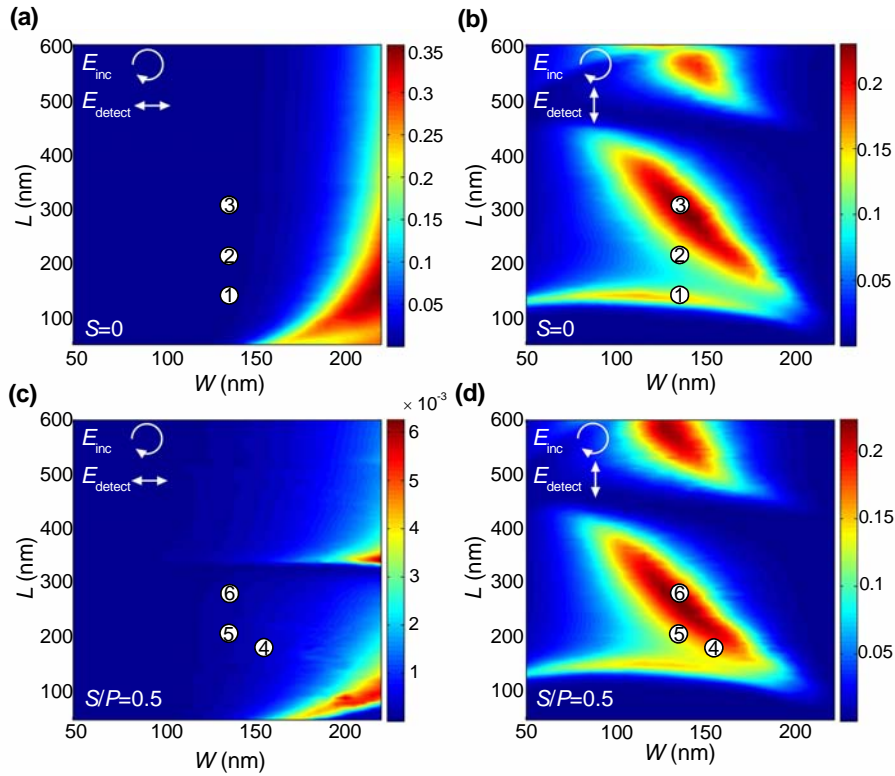


**Figure S3.** Simulated  $x$ -component (a and c) and  $y$ -component (b and d) transmission amplitude of the aligned (a and b) and laterally translated (c and d) dual-layer rectangular nano-apertures as a function of  $L$  and  $W$  when excited with normally incident and circularly polarized light at 900 nm. The lateral translation was fixed at 265 nm. The circles with numbers indicate the values of  $L$  and  $W$  used in the experiments, which correspond to the nanostructures defined in Figure 2a.

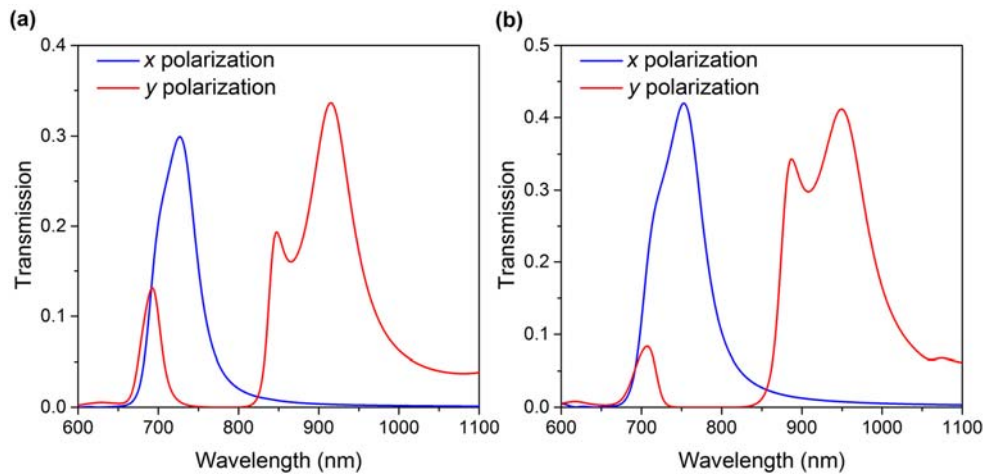


**Figure S4.** Transmission spectra of nano-aperture pair #1 (a) and pair #4 (b) under illumination of  $x$ - and  $y$ -polarized incident light.

### 3. Anomalous refraction in the plasmonic metasurface

When the two layers of nano-apertures are perfectly aligned, **Figures S5a** and **b** show the distribution of the calculated  $E_x$  and  $E_y$  fields in the  $x$ - $z$  plane when a constant phase gradient is created along the  $x$ -direction of the metasurface and the normally incident plane wave is circularly polarized. Note that  $y$ -polarized transmission is steered to an angle consistent with the generalized Snell's law. In contrast, there is minimal  $x$ -polarized transmission which also does not deviate from the normal direction. Slight dislocation of between the two layers of nano-apertures seems to have no significant effect on the performance, as shown in Figures S4 (c-f).

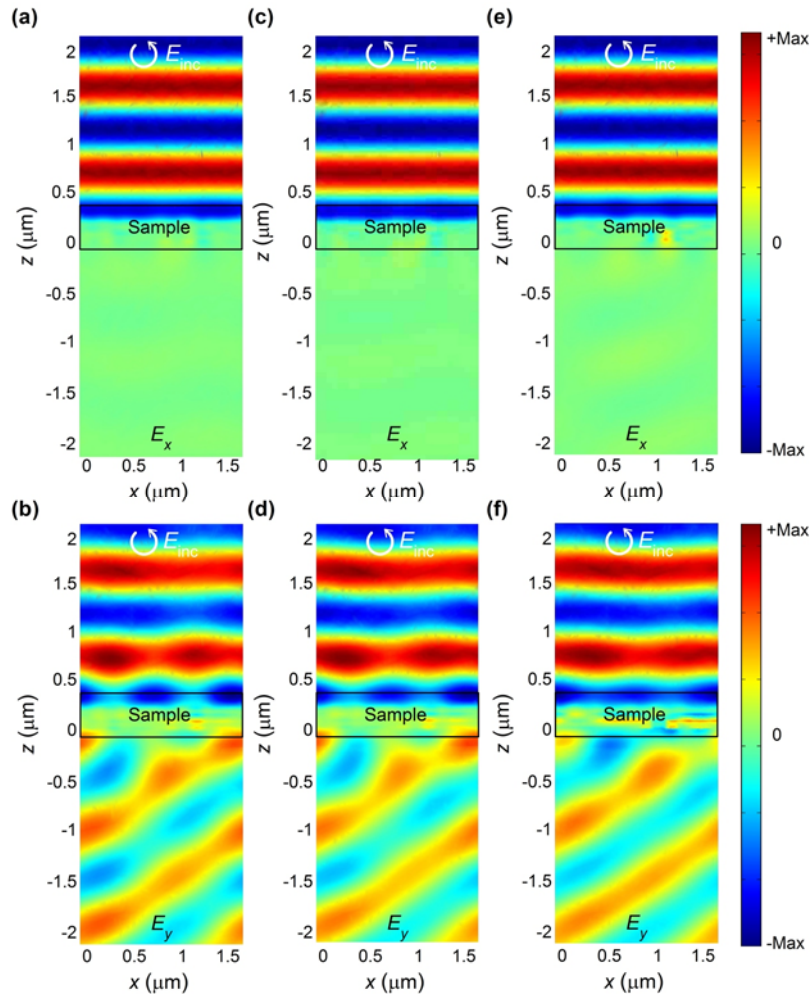


**Figure S5.** Simulated (a, c, e)  $E_x$  and (b, d, f)  $E_y$  field patterns in the  $x$ - $z$  plane, excited by normally circularly polarized incident light at 900 nm, where the dislocations between two layers are (a, b) 0 nm along  $x$ - and  $y$ -axis, (c, d) 50 nm along  $x$ -axis, and (e, f) 50 nm along  $y$ -axis, respectively.

**Figure S6** shows the experimental normalized intensity of the scattered light as a function of observation angle when the metasurface with a linear phase gradient is excited by normally incident and  $y$ -polarized light at various wavelengths.

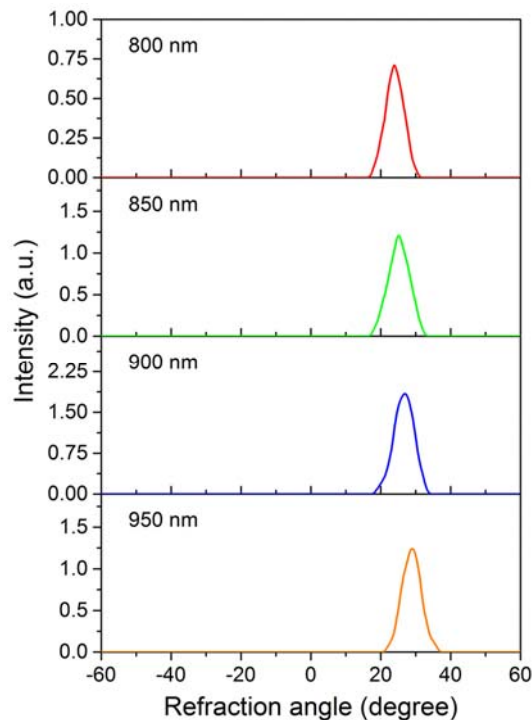


**Figure S6.** Measured far-field intensity at various observation angles for linearly polarized excitations with various wavelengths.

#### 4. Simulation of the generation of vector beams

By simultaneously fully controlling the polarization and phase at the nanoscale, diverse vector optical fields can be generated through the design of appropriate plasmonic metasurfaces. We simulated the generation of the radially and angular polarized beams, and hybrid vector optical beam in **Figure S7**. Figures S7a, b and c show the schematics of simulated modes, which are divided by six regions corresponding to six types of nanostructures. The spatially varying orientation of rectangular nano-apertures in the different regions results to desired distribution of polarization. Figures S7d, e and f show the calculated electric field distributions of the transmission beam.

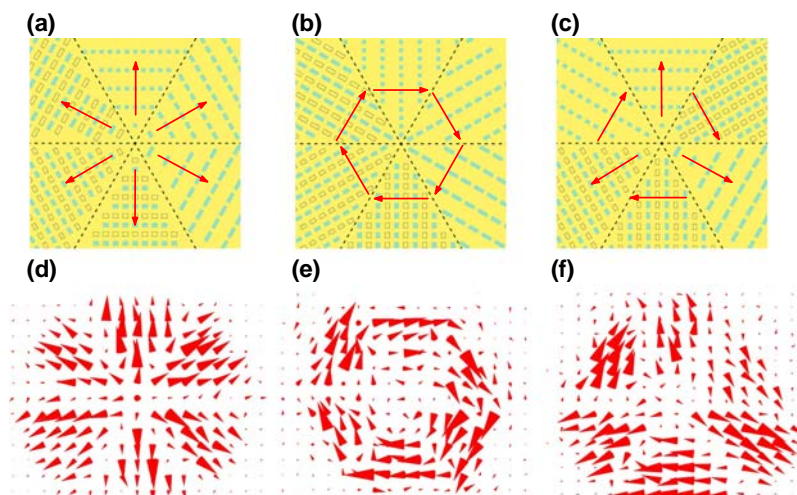


**Figure S7** (a-c) A schematic of the simulated modes for generating the radially, angularly polarized beam and hybrid vector optical beam. The blue and yellow rectangles represent the positions of the nano-apertures in the top and bottom layer, respectively. The arrows indicate the desired distribution of the polarization direction. (d-f) The e-field distribution of the transmitted beam on the cross-section in the propagation direction.

### Movies S1 to S3

Movies S1, S2 and S3 show the e-field oscillation of transmitted beams on the cross-section in the propagation direction, which further demonstrates the generation of the radially, angularly polarized beam and hybrid vector optical beam by the designed plasmonic metasurfaces.